Tuning the magnetotransport behavior of topological insulator with a transition-metal oxide layer

Liyang Liao[1], Peng Chen[2], Xufeng Kou[2], Feng Pan[1] and Cheng Song[1]

[1] Key Laboratory of Advanced Materials (MOE), School of Materials Science and Engineering, Tsinghua University, Beijing 100084, People's Republic of China
[2] School of Information Science and Technology, ShanghaiTech University, Shanghai, 201210 People's Republic of China

E-mail: songcheng@mail.tsinghua.edu.cn

Abstract

The interaction between topological insulator (TI) and its adjacent magnetic layer serves as a basis for exploring the device application of TI. Here we investigate the modulation of the magnetotransport behavior of Bi_2Te_3 TI with a transition-metal oxide layer NiO. It is found that the weak-antilocalization effect is absent at low magnetic fields and the magnetoresistance ratio decreases monotonically with increasing the NiO growth temperature from 300 to 473 K, indicating the suppression of the topological surface states of Bi_2Te_3. Such behaviors are attributed to the decomposition of NiO and the concomitant formation of magnetic impurities at the Bi_2Te_3/NiO interface. Differently, the weak-antilocalization shows no significant weakening with the growth of Cr_2O_3 top layer, due to its better chemical stability. Our observation would be significant for the material selection for the device integration of TI.

(Some figures may appear in colour only in the online journal)

Introduction

Three dimensional topological insulators (TI) are emerging solid-state materials featured as the inverse band structure and topological protected surface states [1–3], which give rise to exotic topological phases and novel phenomena [4–6]. In order to fully explore salient features related to TI, various methods including element doping [6, 7], electric-field control [8], strain engineering [9, 10] and film thickness modulation [11, 12] have been utilized to tailor the nontrivial band structure of topological surface states. Alternatively, combing TI with additional layers into heterostructures or superlattices has been proven to be an effective way to directly couple the topological surface with other physical orders (e.g. ferromagnetism, superconductor, axion electrodynamics) [13–17]. Moreover, due to the abundant material platforms available for the integration, such an approach therefore unfolds new avenues for the TI-based multi-functional applications.

Recent progress focused on the TI heterostructures in which ferromagnetic metal, ferromagnetic insulator and antiferromagnetic semiconductor have been introduced as the adjacent layer [16–20]. For example, a ferromagnetic metal layer can destroy the weak-antilocalization (WAL) feature, suggesting that it could effectively modulate the magnetotransport behaviors of the TI surface states [18]. Meanwhile, ferromagnetic insulator thin films like EuS and YIG are found to induce long-range magnetism into TI through magnetic proximity effect [14, 19, 20]. Recently, antiferromagnetic semiconductors CrSb and MnTe were also reported to introduce robust magnetic order into the adjacent TI layer due to interfacial magnetic exchange couplings [21, 22].

Now the research interest is to investigate TI-based heterostructures with transition-metal oxide (TMO) as the adjacent layer. TMO exhibits many interesting physical properties, e.g. ferromagnetism [23], switchable antiferromagnetism [24], ferroelectricity and magnetoelectric coupling [25], spin

transport [26, 27], and even superconductivity [28], making it appealing to be integrated with TI. In particular, many 3d transition metal oxides hold intricate physical properties mentioned above, and have a simple structure which can be grown at a low temperature, making them especially attractive to be grown on the top of TI. Recently, it is reported that the WAL effect could be suppressed in TI grown on NiO substrate [29], Since the top surface contributes more to transport than the bottom surface [18], it is likely that a stronger modification on transport behavior can be obtained by coupling the adjacent layer to the top surface of TI than to the bottom surface. The experiments below investigate the transport behavior of Bi$_2$Te$_3$ (BT), which is capped by a thin NiO layer grown at different temperatures.

Experiment

High-quality BT sample with a film thickness of 8 nm was grown on Al$_2$O$_3$(0 0 0 1) substrates by monocular beam epitaxy (MBE) at a base pressure of 4×10^{-10} Torr. After growth, the sample was *in situ* passivated by a Te capping layer in order to minimize ambient oxidization. Then the sample was transferred to a magnetic sputtering chamber for the subsequent NiO deposition (the Te capping layer was evaporated at 473 K for 1 h before the NiO growth). To investigate the influence of the growth condition on the magnetotransport behaviors, we prepared 5 nm-thick NiO layer on the BT under the same base pressure of 5×10^{-5} Pa, Ar pressure of 0.4 Pa, and growth rates 0.75 nm min^{-1}, but with different substrate temperatures at 300, 373, and 473 K. The BT/NiO heterostructures were then patterned into Hall bar devices with the channel width of 100 μm and length of 400 μm by photolithography and Ar ion milling. Temperature-dependent magnetotransport was measured in a cryostat from 2.5 to 300 K. The high-resolution transmission electron microscope (HRTEM) images were obtained with focused ion beam (FIB)-prepared cross-sectional samples.

Results and discussion

Figure 1 shows the magnetoresistance ratio $\Delta R/R_0$ of samples BT, BT/NiO (300 K), BT/NiO (373 K) and BT/NiO (473 K) measured at 2.5 K, where R represents the resistance at a certain magnetic field, R_0 denotes the resistance at zero field, and $\Delta R = R - R_0$. For this experiment, the magnetic field was applied perpendicular to the film. For the pure BT sample, a sharp linear cusp appears at low magnetic fields, manifesting the presence of the WAL effect. It is known that the WAL effect is owing to the π Berry phase of the topological surface states in the TI thin film [18]. Bulk state may also have some contribution on the WAL effect, but in our 8 nm TI sample, the 2D surface state contribution should be more important [18]. Using the Hikami–Larkin–Nagaoka (HLN) formula [30, 31], we can evaluate the phase coherence length l_φ and effective 2D surface number characterized by parameter α:
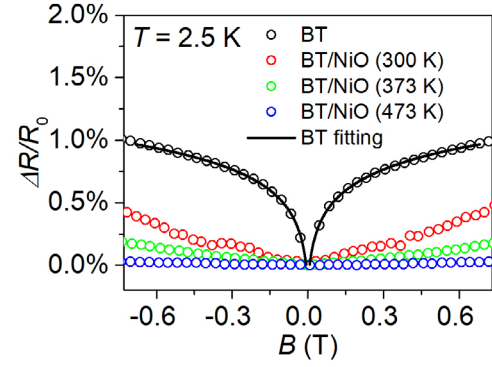

Figure 1. Magnetoresistance for BT and BT/NiO samples with NiO grown at 300 K, 373 K and 473 K. Measurements were carried out at 2.5 K.

$$\Delta\sigma_{2D} = -\frac{\alpha e^2}{2\pi^2\hbar}\left[\ln\frac{\hbar}{4Bel_\varphi^2} - \psi\left(\frac{1}{2} + \frac{\hbar}{4Bel_\varphi^2}\right)\right] \quad (1)$$

where e is the electron charge, B is the applied magnetic field, $\hbar$ is the Planck constant, l_φ is the phase coherent length and $\psi(x)$ is the digamma function. Fitting was done with data from −0.6 T to 0.6 T. The fitting result yields $l_\varphi = 370$ nm and $\alpha = -0.10$, which are consistent with previous reports [18, 32, 33]. Slightly smaller absolute value of α may be due to the heating process during device fabrication, which may cause some oxidation.

The magnetotransport behavior changes dramatically when the top NiO layer is added. Specifically, the magnetoresistance is governed by the conventional parabolic background, and the magnetoresistance ratio is also greatly reduced. These behaviors suggest the topological order protected by time-reversal symmetry is suppressed and a crossover from a symplectic group symmetry to a unitary group symmetry [18, 30]. Remarkably, there is no WAL feature existing for all of the BT/NiO samples grown at different temperatures. Instead, a parabolic magnetoresistance is observed. With increasing growth temperature of NiO, the magnetoresistance ratio decreases monotonically. Corresponding Hall effect curves ($R_\mathrm{H} - B$) are presented in figure 2. For the BT sample (figure 2(a)), the Hall slope R_H/B only changes slightly when the temperature is cooled down from 300 to 2.5 K. Differently, the Hall slope of BT/NiO (473 K) exhibits a strong temperature dependence, as shown in figure 2(b). Also visible is the Hall slope of the BT/NiO (473 K) sample is found to be an order of magnitude smaller than that of the BT sample. It is worth mentioning that the anomalous Hall effect is not observed in all of the samples, which may imply that no robust magnetic impurity-induced ferromagnetic order formed in TI.

According to the Hall slope formula $R_H/B = -1/n \cdot e$ (where n is the 2D carrier density and e is the electron charge), we can calculate the 2D carrier density n based on the Hall curves. The 2D carrier density of BT, BT/NiO (300 K), BT/NiO (373 K) and BT/NiO (473 K) as a function of temperature are summarized in figure 2(c). While the carrier density of BT and BT/NiO (300 K) samples are somehow comparable, approximately
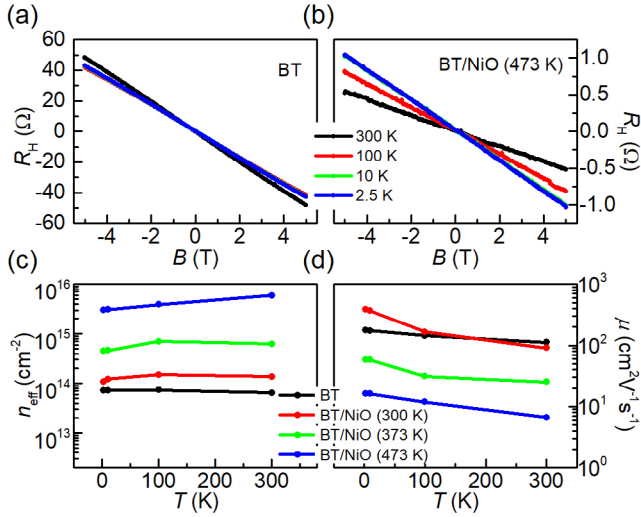
Figure 2. Hall resistance of (a) BT sample and of (b) BT/NiO (473 K) sample at different temperatures. (c) Carrier density for each sample calculated from Hall slope. (d) Mobility for each sample calculated from resistance, device geometry and carrier density.

Figure 3. Kohler's plot for the magnetoresistance curves of (a) BT, (b) BT/NiO (300 K), (c) BT/NiO (373 K), and (d) BT/NiO (473 K) samples.

10^{14} cm^{-2}, the BT/NiO (373 K) and BT/NiO (473 K) samples have much higher carrier density. For all of the three BT/NiO samples, the carrier density increases with increasing growth temperature. The calculated mobility μ for all of the samples are displayed in figure 2(d). Similar to the carrier density case, BT and BT/NiO (300 K) samples exhibit similar mobility of several hundreds of cm^2 V^{-1} s^{-1}, which is quite characteristic for TI films, while the two samples grown at higher NiO temperatures have much lower mobility. For three BT/NiO samples, the mobility decreases with increasing NiO growth temperature. The rise of carrier density and the decline of mobility with higher NiO growth temperature suggest that the impurity concentration increases with increasing NiO growth temperature.

The magnetoresistance of BT, BT/NiO (300 K), BT/NiO (373 K) and BT/NiO (473 K) samples at different temperatures also supports this relationship between impurity concentration and NiO growth temperature. Corresponding data are illustrated in figure 3. We use a Kohler's Plot, i.e. a $\Delta R/R_0$ versus B/R_0 plot, to compare the magnetoresistance of the samples, where the 2.5 K data is obtained from the same raw data as figure 1. According to the Kohler's Rule, for a single-band metal with only one kind of carriers, the magnetoresistance ratio $\Delta R/R_0$ is the function of B/R_0 [34]. In this case, it is expected that the Kohler's plots should overlap onto a single curve at different temperatures. All of the curves are obtained from raw magnetoresistance data from −5 T to 5 T. Before plotting the Kohler's graph of BT sample, we deducted the contribution of WAL term using HLN formula fitting from −0.6 T to 0.6 T. The result yields that after deducting the WAL contribution, the BT sample approximately obeys the Kohler's rule (figure 3(a)). The BT/NiO (300 K) sample also approximately obeys the Kohler's rule (figure 3(b)). In contrast, the BT/NiO (373 K) (figure 3(c)) and BT/NiO (473 K) (figure 3(d)) samples show a clear deviation from the Kohler's
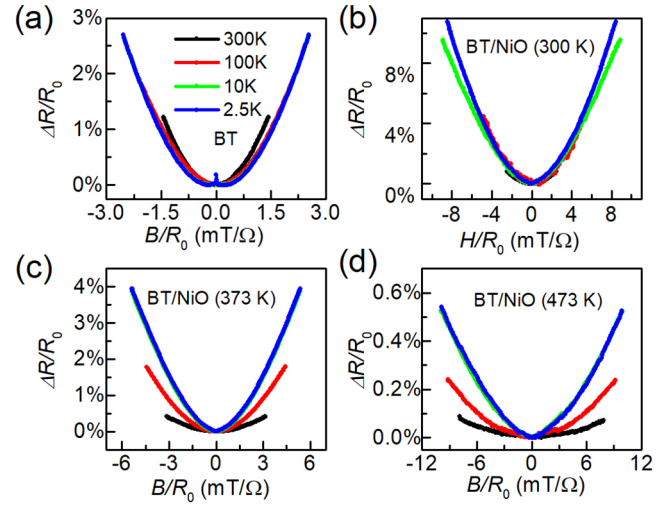
Rule. These results reveal that different kinds of carriers or different scattering mechanisms may exist in the transport in the BT/NiO samples grown at higher NiO temperatures. It can also be seen in the Hall measurement (figure 2(c)) that the calculated carrier density of BT/NiO (373 K) and BT/NiO (473 K) change with temperature, coinciding with the Kohler's plot. Both phenomena are related to the impurity concentration introduced in the growth process.

The decomposition of NiO during the growth may play an important role on the transport behavior [35]. In particular, the decomposition would produce metallic Ni at the interface, which can be detected by x-ray photoelectron spectroscopy (XPS). Given that the XPS can only characterize the elements with several nanometers depth from the sample surface, we thus grew additional BT/NiO samples with the NiO thicknesses from 0.25 to 5 nm at 300 K. Note that the Ni peak at 852.8 eV [36, 37] emerges in the Ni $2p_{3/2}$ spectroscopy in the BT/NiO (0.25 nm) sample (figure 4(a)), and the fitting confirms that the Ni atom ratio between in Ni metal form to in NiO form is Ni^0: Ni^{2+} = 0.1: 1. For the BT/NiO (0.5 nm) sample, the Ni peak still exists but much weaker (figure 4(b)), giving rise to Ni^0: Ni^{2+} = 0.022: 1. For the BT/NiO (1.5 nm) and BT/NiO (5 nm) samples, as presented in figures 4(c) and (d), respectively, data can be fitted well when considering NiO only [38]. These observations indicate that metallic Ni exists at the BT/NiO interface, while the amount of metallic Ni is rather small, thus it is unlikely to form a continuous metallic Ni layer on the top of TI.

HRTEM was used to directly probe the interfacial state of the BT/NiO heterostructure samples. Concomitant cross-section HRTEM images of BT/NiO (300 K) and BT/NiO (473 K) samples are shown in figures 5(a) and (b), respectively. Remarkably, the BT/NiO (300 K) sample exhibits a well-defined BT/NiO interface, and the NiO layer is polycrystalline. On the contrary, in the BT/NiO (473 K) sample, the BT/NiO interface is rough with clear mixing features, and the NiO layer shows an obvious amorphous tendency. A comparison
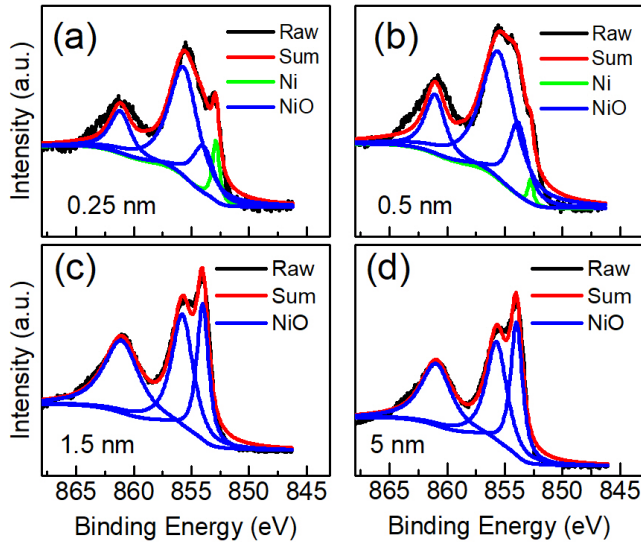
Figure 4. XPS Ni $2p_{3/2}$ spectra of BT/NiO samples with the NiO thickness of 0.25 nm (a), 0.5 nm (b), 1.5 nm (c) and 5 nm (d) grown at 300 K.
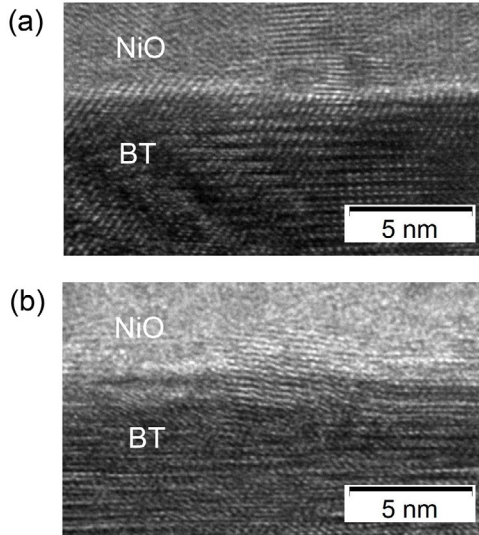

Figure 5. Cross-sectional HRTEM images for (a) BT/NiO (300 K) and (b) for BT/NiO (473 K) samples.

of these two HRTEM images reflects that the higher growth temperature (473 K) not only advances the interdiffusion at the BT/NiO interface, but also reduces the crystallinity of the NiO layer. Combining the transport results and the HRTEM observations, we conclude that at high growth temperature, the decomposition of NiO has a more serious effect on the structure, and hence the transport behavior of the heterostructure.

It is a question that whether other TMO would also disturb the transport behavior of TI via similar mechanism. A control experiment was conducted by growing 5 nm-thick Cr_2O_3 on the top of the BT sample by radio frequency sputtering at 473 K. Identical film growth process and measurements were used as the NiO case. In the Ellingham graph [39], the line of Cr_2O_3 is under that of NiO, reflecting better chemical stability of Cr_2O_3, thus decomposition of Cr_2O_3 is more difficult to occur. The results for the BT/Cr_2O_3 sample are displayed in figure 6.
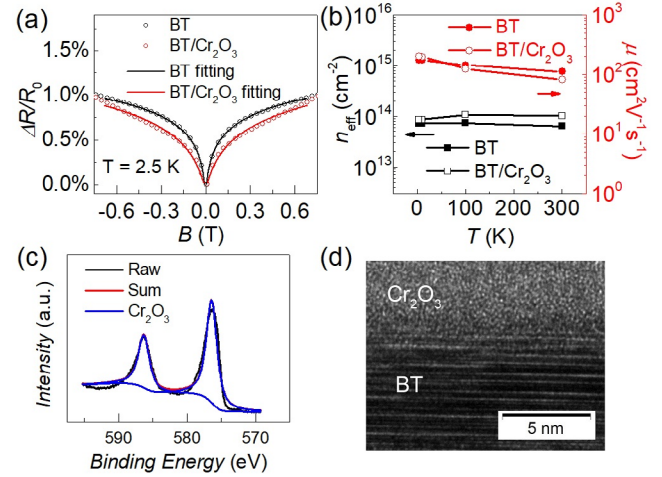

Figure 6. (a) Magnetoresistance curve of BT/Cr_2O_3 sample at 2.5 K denoted by symbols and corresponding fitting curves denoted by line. Magnetoresistance curve of BT sample at 2.5 K and its fitting curve are also plotted for a comparison. (b) Carrier density and mobility of BT and BT/Cr_2O_3 samples at different temperatures. Plot scale is the same as in figure 2. (c) XPS Cr 2p spectra of BT/Cr_2O_3 sample. (d) Cross-sectional HRTEM image for BT/Cr_2O_3 sample.

The obtained magnetoresistance curve also shows the WAL feature (figure 6(a)), in contrast to the absence of WAL for the BT/NiO (473 K) sample. The fitting of the HLN formula gives $l_\varphi = 163$ nm and $\alpha = -0.17$. Although the absolute value of α and the coherent length are slightly smaller than other WAL works in TI, they are still comparable [18, 29, 32], indicating that no significant suppression is caused by Cr_2O_3 on the WAL effect. On the other hand, both the carrier density and mobility of the BT/Cr_2O_3 sample are comparable to those of the BT sample (figure 6(b)). Meanwhile, XPS data show Cr $2p_{3/2}$ peak at 576.4 eV and Cr $2p_{1/2}$ peak at 586.3 eV (figure 6(c)), which is the typical signature of Cr^{3+} in Cr_2O_3 [40, 41]. There is no peak corresponding to metallic Cr. These results demonstrate that although the growth temperature of Cr_2O_3 layer is as high as 473 K, owing to the chemical stability of Cr_2O_3, no strong decomposition occurs and few magnetic impurities form at the interface. However, the HRTEM image shown in figure 6(d) indicates amorphous tendency similar to the BT/NiO (473 K) sample, suggests that the high growth temperature is more likely to do harm to the crystal quality of TMO on TI.

We then propose a phenomenological model to explain the underlying physics in our heterostructure samples. Figure 7(a) illustrates the schematic of a BT/NiO heterostructure, where the NiO layer is grown at comparatively low temperature, e.g. 300 K. Due to the poor chemical stability of NiO, it decomposes in growth process, and forms a small amount Ni atoms and/or particles. Also, decomposed oxygen could diffuse slightly into the BT layer, where oxidation occurs simultaneously. Nevertheless the comparatively low temperature cannot provide enough energy for the Ni and oxygen atoms to diffuse deep into the BT layer. In this scenario, the Ni atoms and/or particles would act as interfacial impurities, which destroys the topological surface state, but do not induce a
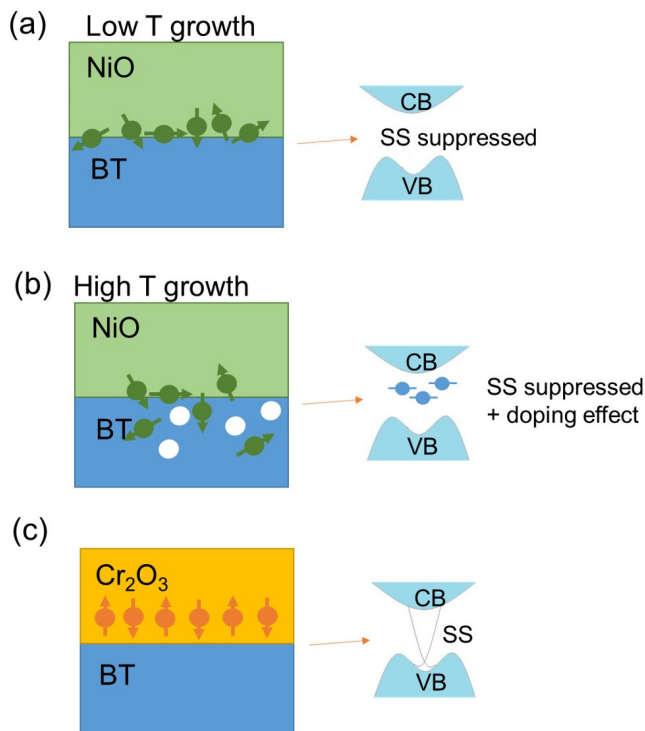
Figure 7. Schematic of TI/transition metal oxide heterostructure in this work. CB, conductive band; VB, valence band; SS, surface state. (a) In BT/NiO sample with low growth temperature (*T*), decomposition of NiO in growth process leads to the formation of small amount Ni atoms and/or particles as magnetic impurities, which suppresses the surface state. (b) In the BT/NiO sample with high growth temperatures, Ni and O atoms formed by the decomposition of NiO can diffuse into BT and formed impurity energy level. While the surface state is suppressed by the magnetism of Ni, the bulk state also suffers doping effect. (c) In BT/Cr$_2$O$_3$ sample, owing to better chemical stability of Cr$_2$O$_3$, no severe decomposition happens and the surface state is preserved.

strong doping effect. When the growth temperature increases, the decomposition of NiO becomes more serious, and the impurities could gain more energy to diffuse deep into the TI, as displayed in figure 7(b). The impurity concentration would rise accordingly. In this case, the surface state is strongly suppressed, and the bulk state also suffers doping effect, characterized by the increase of carrier density and the decline of mobility. Since the magnetoresistance ratio is approximately equal to $1 + (\mu B)^2$ [18], the decline of mobility also explains the reduced magnetoresistance ratio. Differently, because of the high chemical stability of Cr$_2$O$_3$ [39], the decomposition issue is greatly alleviated in the BT/Cr$_2$O$_3$ heterostructure, thus the surface state was preserved, followed by the observed WAL effect.

Conclusion

We studied the transport behavior of TI/TMO heterostructure in which the TMO layer was deposited on the top of TI. For BT/NiO heterostructure, WAL effect is totally suppressed when the NiO growth temperature ranges from 300 K to 473 K, which is attributed to the decomposition of NiO during growth and the resulting formation of magnetic impurities. These magnetic impurities suppressed the surface state of BT, leading to the absence of WAL effect. When the NiO growth temperature increases, the decomposed product diffuses into BT and causes doping effect. Hence, the carrier density increases, the mobility and the parabolic magnetoresistance ratio declines monotonically with increasing growth temperature. But for BT/Cr$_2$O$_3$ heterostructure, in which the TMO layer is more stable, the WAL effect is preserved, the carrier density and the mobility are comparable with BT sample even when the growing temperature was as high as 473 K. Our findings suggest TMO can be a potential material for manipulating the electronic state and transport behavior of TI, and the chemical stability of the selected TMO materials as well as the processing temperature can significantly affect the transport performance of the BT/TMO heterostructure.

ORCID iDs

Feng Pan https://orcid.org/0000-0002-3788-7894
Cheng Song https://orcid.org/0000-0002-7651-9031

References

[1] Zhang H, Liu C-X, Qi X-L, Dai X, Fang Z and Zhang S-C 2009 *Nat. Phys.* **5** 438
[2] Hasan M Z and Kane C L 2010 *Rev. Mod. Phys.* **82** 3045
[3] Qi X-L and Zhang S-C 2011 *Rev. Mod. Phys.* **83** 1057
[4] Liu C-X, Zhang H, Yan B, Qi X-L, Frauenheim T, Dai X, Fang Z and Zhang S-C 2010 *Phys. Rev.* B **81** 041307
[5] Yu R, Zhang W, Zhang H-J, Zhang S-C, Dai X and Fang Z 2010 *Science* **329** 61–4
[6] Chang C-Z *et al* 2013 *Science* **340** 167
[7] Babakiray S, Holcomb M B and Lederman D 2016 *J. Phys.: Condens. Matter* **28** 165601
[8] Fan Y *et al* 2016 *Nat. Nanotechnol.* **11** 352–9
[9] Kozlov D A, Kvon Z D, Olshanetsky E B, Mikhailov N N, Dvoretsky S A and Weiss D 2014 *Phys. Rev. Lett.* **112** 196801
[10] Dantscher K M *et al* 2015 *Phys. Rev.* B **92** 165314
[11] Glinka Y D, Babakiray S, Johnson T A and Lederman D 2015 *J. Phys.: Condens. Matter* **27** 052203
[12] Zhang Y *et al* 2010 *Nat. Phys.* **6** 584

[13] Vobornik I, Manju U, Fujii J, Borgatti F, Torelli P, Krizmancic D, Hor Y S, Cava R J and Panaccione G 2011 *Nano Lett.* **11** 4079–82

[14] Lang M *et al* 2014 *Nano Lett.* **14** 3459–65

[15] Fu L and Kane C L 2008 *Phys. Rev. Lett.* **100** 096407

[16] Xu J-P *et al* 2015 *Phys. Rev. Lett.* **114** 017001

[17] Mogi M, Kawamura M, Yoshimi R, Tsukazaki A, Kozuka Y, Shirakawa N, Takahashi K S, Kawasaki M and Tokura Y 2017 *Nat. Mater.* **16** 516

[18] He H T, Wang G, Zhang T, Sou I K, Wong G K, Wang J N, Lu H Z, Shen S Q and Zhang F C 2011 *Phys. Rev. Lett.* **106** 166805

[19] Tang C *et al* 2017 *Sci. Adv.* **3** e1700307

[20] Katmis F *et al* 2016 *Nature* **533** 513–6

[21] He Q L *et al* 2018 *Phys. Rev. Lett.* **121** 096802

[22] He Q L *et al* 2018 *Nat. Commun.* **9** 2767

[23] Kämper K P, Schmitt W, Güntherodt G, Gambino R J and Ruf R 1987 *Phys. Rev. Lett.* **59** 2788–91

[24] Chen X Z *et al* 2018 *Phys. Rev. Lett.* **120** 207204

[25] Rado G T and Folen V J 1961 *Phys. Rev. Lett.* **7** 310–11

[26] Hou D, Qiu Z, Barker J, Sato K, Yamamoto K, Vélez S, Gomez-Perez J M, Hueso L E, Casanova F and Saitoh E 2017 *Phys. Rev. Lett.* **118** 147202

[27] Qiu Z, Hou D, Barker J, Yamamoto K, Gomonay O and Saitoh E 2018 *Nat. Mater.* **17** 577–580

[28] Takada K, Sakurai H, Takayama-Muromachi E, Izumi F, Dilanian R A and Sasaki T 2003 *Nature* **422** 53–55

[29] Bhowmick T, Jerng S K, Jeon J H, Roy S B, Kim Y H, Seo J, Kim J S and Chun S H 2017 *Nanoscale* **9** 844–9

[30] Hikami S, Larkin A I and Nagaoka Y 1980 *Prog. Theor. Phys.* **63** 707–10

[31] McCann E, Kechedzhi K, Fal'ko V I, Suzuura H, Ando T and Altshuler B L 2006 *Phys. Rev. Lett.* **97** 146805

[32] Chen J *et al* 2010 *Phys. Rev. Lett.* **105** 176602

[33] Nandi D *et al* 2018 *Phys. Rev.* B **98** 214203

[34] Chan M K, Veit M J, Dorow C J, Ge Y, Li Y, Tabis W, Tang Y, Zhao X, Barišić N and Greven M 2014 *Phys. Rev. Lett.* **113** 177005

[35] Jang W L, Lu Y M, Hwang W S, Dong C L, Hsieh P H, Chen C L, Chan T S and Lee J F 2011 *Europhys. Lett.* **96** 37009

[36] Biesinger M C, Payne B P, Lau L W M, Gerson A and Smart R S C 2009 *Surf. Interface anal.* **41** 324

[37] Payne B P, Biesinger M C and McIntyre N S 2012 *J. Electron Spectrosc. Relat. Phenom.* **185** 159

[38] Mansour A N 1994 *Surf. Sci. Spectra* **3** 231

[39] Ellingham H J T 1944 *J. Soc. Chem. Ind.* **63** 125

[40] Desimoni E, Malitesta C, Zambonin P G and Rivière J C 1988 *Surf. Interface Anal.* **13** 173

[41] Zhang W S, Brück E, Zhang Z D, Tegus O, Li W F, Si P Z, Geng D Y and Buschow K H J 2005 *Physica* B **358** 332